


RESEARCH ARTICLE | SEPTEMBER 06 2023

Efficient global sensitivity analysis of kinetic Monte Carlo simulations using Cramér–von Mises distance

Sina Dortaj ; Sebastian Matera  



J. Chem. Phys. 159, 094110 (2023)

<https://doi.org/10.1063/5.0160873>

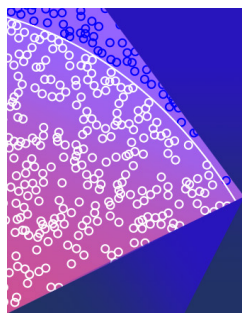


View
Online



Export
Citation

CrossMark



The Journal of Chemical Physics

Special Topic: Monte Carlo methods,
70 years after Metropolis *et al.* (1953)

Submit Today

Efficient global sensitivity analysis of kinetic Monte Carlo simulations using Cramér–von Mises distance

Cite as: J. Chem. Phys. 159, 094110 (2023); doi: 10.1063/5.0160873

Submitted: 6 June 2023 • Accepted: 11 August 2023 •

Published Online: 6 September 2023



View Online



Export Citation



CrossMark

Sina Dortaj^{1,2,a)}  and Sebastian Matera^{1,2,b)} 

AFFILIATIONS

¹Fritz-Haber-Institut der Max-Planck-Gesellschaft, Faradayweg 4-6, 14195 Berlin, Germany

²Institut für Mathematik, Freie Universität Berlin, Arnimallee 6, 14195 Berlin, Germany

^{a)}Electronic mail: dortaj.sina@gmail.com

^{b)}Author to whom correspondence should be addressed: matera@math.fu-berlin.de

ABSTRACT

Typically, the parameters entering a physical simulation model carry some kind of uncertainty, e.g., due to the intrinsic approximations in a higher fidelity theory from which they have been obtained. Global sensitivity analysis (GSA) targets quantifying which parameter uncertainties impact the accuracy of the simulation results, e.g., to identify which parameters need to be determined more accurately. We present a GSA approach based on the Cramér–von Mises distance. Unlike prevalent approaches, it combines the following properties: (i) it is equally suited for deterministic as well as stochastic model outputs, (ii) it does not require gradients, and (iii) it can be estimated from numerical quadrature without further numerical approximations. Using quasi-Monte Carlo for numerical integration and a first-principles kinetic Monte Carlo model for the CO oxidation on RuO₂(110), we examine the performance of the approach. We find that the results agree very well with what is known in the literature about the sensitivity of this model and that the approach converges in a modest number of quadrature points. Furthermore, it appears to be robust against even extreme relative noise. All these properties make the method particularly suited for expensive (kinetic) Monte Carlo models because we can reduce the number of simulations as well as the target variance of each of these.

Published under an exclusive license by AIP Publishing. <https://doi.org/10.1063/5.0160873>

I. INTRODUCTION

Most models of physicochemical behavior depend on a number of parameters, which are characteristic of the problem we want to describe. Typically, these parameters carry a non-negligible uncertainty or variability. This might result from the actual problem setting. For instance, in materials screening, we are interested in the behavior of a class of materials, where the particular choice of the parameter values distinguishes between different materials in that class. Even for one particular material, we typically know the parameter values only approximately as these need to be determined from either experimental data or from higher fidelity models, e.g., quantum chemical methods. In these cases, parameter uncertainty arises either due to the unavoidable noise on experimental data or due to the intrinsic approximations in the high-fidelity model. Consequently, the model's output is uncertain itself, and it is of interest which parameter uncertainties are most responsible for this

variability. Such sensitivity information would allow for a purposeful distribution of resources by a more accurate determination of only the most important parameters or a qualitative interpretation of the crucial factors controlling the behavior of a material class.

In the context of chemical kinetics, the uncertainties can be assigned to the reaction energies and barriers or the rate constants, respectively. Here, the sensitivity information is closely related to the notion of rate-determining steps (RDS). Commonly, RDSs are determined by local sensitivity analyses (LSAs), i.e., by the gradient of the model output at the default parameter values.^{1,2} However, the intrinsic linear approximation behind LSA is only appropriate for typically highly nonlinear kinetic models if the parameter uncertainties are small. Global sensitivity analyses (GSAs) overcome this problem by sampling the parameter space according to the error distribution and thereby the nonlinear response. Such analyses have been applied to numerous mean-field microkinetic models.^{3–5} In contrast, there exist only very few studies of GSA for

the more accurate kinetic Monte Carlo (kMC) models^{6,7} as established GSA approaches require complex sampling strategies of the parameter domain, kMC simulations are comparatively costly, and their numerical error converges only slowly.

We present a novel approach to GSA based on the Cramér–von Mises (CvM) distance, which, while being generally applicable, is particularly suited for the use with kMC and other Monte Carlo models. This approach requires neither any gradient information, which is notoriously difficult to estimate from kMC simulations, nor a specialized sampling strategy for the parameter space or surrogate models. Instead, almost any numerical integration method can be employed, and with a suitable integration method, reasonably accurate sensitivity index estimates can be obtained with only a modest number of kMC simulations. Moreover, the approach seems to be rather robust against the noise in the kMC estimates, and therefore, every kMC simulation can be run with a modest computational footprint. Using quasi-Monte Carlo integration for the parameter space, we demonstrate this on a first-principles kinetic Monte Carlo (1p-kMC) model for CO oxidation on RuO₂(110).⁸ Such models have attracted much attention during the last years because of their predictive quality.^{9,10} The downside is the relatively high error of ~0.2 eV for the underlying density functional theory derived energetics.¹¹ This error accounts for uncertainties of orders of magnitude for the rate constants at typical temperatures. For these large uncertainties, LSA might provide only limited insight or even misleading results,¹² and GSA will be a more appropriate choice.

II. UNCERTAINTY MODELING AND GLOBAL SENSITIVITY ANALYSIS

The goal of every GSA is to determine a set of numbers, the sensitivity indices (SInds), which quantify how strongly the output y of a model depends on the different input parameters. The model itself can be characterized by the conditional distribution of the output y , given the parameters values $\mathbf{x} \in \mathbb{R}^D$, represented by its cumulative distribution function (CDF) $F(y|\mathbf{x})$. For the methodology below, no explicit knowledge of this distribution is required but only a computational model that draws samples from $F(y|\mathbf{x})$ for given parameters \mathbf{x} , e.g., a kMC simulation. In general, this allows the treatment of stochastic outputs, of which deterministic input–output relations are a special case.

Next to the model itself, we need a probability distribution [CDF $F(\mathbf{x})$] of the input parameters \mathbf{x} , which represents the uncertainty of \mathbf{x} . This distribution must be interpreted in an information theoretical setting, i.e., it represents our knowledge about the values of the parameters. For instance, if we can determine a parameter directly from an experiment, there will be an unavoidable noise in the experimental data, and we would repeat this several times to average out this noise and estimate the standard deviation. Then, by the central limit theorem, we would expect that this average will be Gaussian distributed. In contrast, the parameters might have been determined from a high-fidelity model by some numerical method for which we have error bounds. We would then employ a uniform distribution between these bounds because this would maximize the entropy of the distribution. In the context of 1p-kMC, the error primarily originates from the modeling assumptions in the employed density functional, which is none of the above-mentioned cases.

However, for adsorption energies and barriers in heterogeneous catalysis, it is commonly assumed that the employed functionals in the generalized gradient approximation produce errors, which are not much worse than 0.2 eV.¹¹

From $F(y|\mathbf{x})$ and $F(\mathbf{x})$, we form the joint distribution of output and input [CDF $F(y, \mathbf{x})$]. Our approach to GSA is based on analyzing the joint marginal distribution of the output y and only one input parameter x_i [CDF $F(y, x_i)$], that is, the distribution of y and x_i after averaging over all remaining input parameters. This will be compared to the marginal distribution of only y [CDF $F(y)$] and the marginal distribution of only x_i [CDF $F(x_i)$]. For later use in computations, it is useful to express the CDFs in terms of integrals over the probability measure $dF(y, \mathbf{x})$ of the non-marginal distribution $F(y, \mathbf{x})$ of output and all inputs. Since $F(y)$ is nothing than the probability for the output to be below the value y , this is given by

$$F(y) = \int_{-\infty}^y dF(y') \\ = \int H(y - y') dF(y') = \int H(y - y') dF(y', \mathbf{x}'), \quad (1)$$

where $H(\cdot)$ is the Heaviside step function. Here, we exploited that the marginal measure $dF(y)$ can be obtained from the joint measure $dF(y, \mathbf{x})$ by integrating over \mathbf{x} . Using the same arguments, the CDF $F(x_i)$ is given by

$$F(x_i) = \int H(x_i - x'_i) dF(y', \mathbf{x}'). \quad (2)$$

The joint marginal CDF, $F(y, x_i)$, is simply the probability that the output is below y and the i th input is below x_i . In terms of Heaviside functions, this means

$$F(y, x_i) = \int H(x_i - x'_i) H(y - y') dF(y', \mathbf{x}'). \quad (3)$$

We will employ Eqs. (1)–(3) to formulate the global sensitivity measure and an estimator for it. The goal of GSA is to identify those parameters that uncertainty has the most impact on the uncertainty of the output. If a parameter x_i is unimportant, that means the output y is statistically independent of this parameter. The idea behind our and other distribution-based approaches to GSA³ is to measure the statistical dependence of these two random variables. In terms of distributions, statistical independence means that the joint marginal distribution is of product form and its CDF, $F_{s.t.}(y, x_i)$, obeys

$$F_{s.t.}(y, x_i) = F(x_i)F(y), \quad (4)$$

where $F(y)$ and $F(x_i)$ are the marginal distribution of the output y , Eq. (1), and the i th input x_i , Eq. (2). If we have a significant statistical dependence between y and x_i , the true joint marginal distribution $F(y, x_i)$, Eq. (3), will strongly deviate from this product form $F_{s.t.}(y, x_i)$. Therefore, we will base the SInd, S_i , on some distance measure between these two distributions, for which we will employ the Cramér–von Mises distance D_i (CvM).¹³ We define the SInd S_i by

$$D_i = \int |F(y, x_i) - F(x_i)F(y)|^2 dF(y, \mathbf{x}), \\ S_i := \frac{D_i}{\sum_j D_j}, \quad (5)$$

where the normalization of the CvM ensures that all S_i add up to one, as is the case for the degree of rate control.¹⁴

At this point, there is nothing special about the CvM-based GSA (CvM-GSA). Any other distance measure between probability distributions would define a similarly valid SInd, e.g., the already employed total variation.¹⁵ The benefit of the CvM is in more practical terms as it can directly be estimated from numerical integration without any further approximation. For this, we assume that we have a numerical rule for integrating over of the input variables with N nodes $\{\mathbf{x}_n\}_{n=1}^N$ and weights $\{w_n\}_{n=1}^N$ for which

$$\sum_{n=1}^N w_n = 1, \quad (6)$$

$$\lim_{N \rightarrow \infty} \sum_{n=1}^N t(\mathbf{x}_n) w_n = \int t(\mathbf{x}) dF(\mathbf{x}), \quad (7)$$

$$\lim_{N \rightarrow \infty} |w_n|^2 = 0 \quad (8)$$

for a function t , which can be discontinuous. The properties (6) and (7) are minimal requirements for a numerical quadrature rule, whereas Eq. (8) holds for many practical rules, but it is easy to construct a valid quadrature rule that violates this.

With this rule, we now approximate the CDFs (1)–(3),

$$\tilde{F}_N(y) = \sum_{n=0}^N w_n H(y - y_n), \quad (9)$$

$$F_N(x_i) = \sum_{n=0}^N w_n H(x_i - x_{i,n}), \quad (10)$$

$$\tilde{F}_N(y, x_i) = \sum_{n=0}^N w_n H(y - y_n) H(x_i - x_{i,n}), \quad (11)$$

where y_n is a single sample drawn from $F(y|\mathbf{x}_n)$ by the use of our model. For Eqs. (9)–(11), we first rewrote $\int \dots dF(y', \mathbf{x}') = \int \dots dF(y'|\mathbf{x}') dF(\mathbf{x}')$. Then, we discretized the integration over x , which left us with the conditional integrals $\int \dots dF(y'|\mathbf{x}_n)$. Without explicit knowledge of $F(y|\mathbf{x})$, these integrals must be approximated using samples drawn by our model. By Eq. (8), it now suffices to draw only a single sample y_n per node \mathbf{x}_n for (9)–(11) to converge to the true CDFs. For the deterministic case, where y is a function of \mathbf{x} , this is obviously true because all samples would take the same value [and the constraint (8) can be dropped]. For the general stochastic case, the constraint (8) ensures that the sampling noise averages out in the limit $N \rightarrow \infty$. For details, we refer to the Appendix.

We now take the approximate CDFs (9)–(11) and insert them into the definition of the CvM. We then conduct the same steps as for obtaining (9)–(11). This results in the estimator for the CvM,

$$D_i \approx \sum_{m=1}^N w_m \left| \left(\sum_{n=1}^N h_{i,mm}^{(x)} h_{mn}^{(y)} w_n \right) - \left(\sum_{n=1}^N h_{i,mm}^{(x)} w_n \right) \left(\sum_{n=1}^N h_{mn}^{(y)} w_n \right) \right|^2, \quad (12)$$

with $h_{i,mm}^{(x)} = H(x_{i,m} - x_{i,n})$ and $h_{mn}^{(y)} = H(y_m - y_n)$.

Estimating the CvM thus requires only choosing a quadrature rule and running the model once for each node. From these data, we can calculate all SInds of the input variables. The downside of CvM-GSA is that the SInd from CvM-GSA has no intuitive interpretation as other approaches, such as variance-based GSA,¹⁶ Wasserstein metric-based GSA (W-GSA),¹² or gradient-based GSA.¹⁷ However, compared with other existing approaches, the CvM-GSA has several advantages. Unlike gradient-based GSA, it does not require derivative information, which can be demanding to estimate from Monte Carlo simulations.³ GSA based on an Analysis Of Variances (ANOVA) also is derivative-free.¹⁶ However, this requires either a surrogate model, which can be demanding to obtain especially when dealing with dozens of parameters and non-smooth input–output relations,^{7,12} or a specialized parameter sampling strategy is needed with an extra dataset for each SInd.¹⁸ Both become computationally inefficient if the parameter space is high-dimensional. The CvM has also been applied to generalize the ANOVA-based GSA.¹⁹ While this approach can generally address more complex questions than our CvM-GSA, it also requires similar sampling strategies as the ANOVA-based approach. As the CvM-GSA, other distribution-based approaches do not require a deterministic input–output relation and can work on only a single dataset to estimate all SInds and no surrogate.^{6,15} However, these approaches require some kind of random quadrature, and they achieve the single dataset property only by introducing additional numerical approximations. In contrast, the quadrature rule is the only source of error for the CvM-based approach, and we can employ (almost) arbitrary quadrature rules.

Besides these properties, the CvM-GSA is invariant with respect to monotone component-wise transformations of y and \mathbf{x} . This is not the case for gradient-based GSA, which is neither invariant with respect to a transformation of the output y nor a transformation of the input \mathbf{x} . In particular, the latter is problematic because the GSA will assign different importance to the, in principle, same parameter depending on how we choose to represent this, e.g., linear against logarithmic representation. However, in both representations, we have the same uncertainty encoded by the transformed probability distribution, and thus, the importance of a certain parameter should be invariant. Variance-based GSA, but also our W-GSA, is invariant under the componentwise monotone transformation of the input, but not for the output. Whether this is a disadvantage or not depends on the application, where a certain representation might have been established for interpretation purposes. However, we have the problem that two transformations of the output might give contradicting results, and it requires expert knowledge to decide which one is correct. Completely invariant approaches, such as the CvM-GSA and the total variation GSA, remove this ambiguity. Loosely speaking, such approaches provide a balanced representation assigning those subdomains of the joint input–output space a higher importance for the sensitivity, where most of the probability is located. Non-invariant approaches are instead prone to be dominated by outlier domains, where the output takes large absolute values, even though the probability for such values can be extremely low. Another advantage of this invariance is again in practical terms. We can simply choose the transformation such that we obtain a good numerical performance. For instance, the logarithm of the turnover frequency (TOF) is typically considered in catalysis, especially in the setting of first principles kMC because of the high parametric uncertainty.

Therefore, it would make sense to consider the sensitivity of this logarithm. However, in practice, a kMC might return zero for the TOF for some parameter settings due to a too short kMC trajectory, even though the real TOF will typically be larger than zero (albeit very small). The logarithm is then not defined, and the GSA must fail. Because of the invariance of the CvM, we can work on a linear scale, and a zero TOF is unproblematic.

The dimensionality of typical microkinetic models is in the order of a few tens, and classical integration approaches will suffer from the curse of dimensionality. For problems where $F(\mathbf{x})$ can be mapped onto a uniform distribution on a hypercube, Quasi-Monte Carlo (QMC) approaches²⁰ likely are the best choice for numerical integration over the parameter domain. This is because they provide a good balance between the sampling and the numerical error, i.e., the error due to the use of only a finite number of samples per node and the error that comes from the discretization in the parameter domain. First, QMC are equal weight quadrature rules as classical Monte Carlo integration. Among all possibilities, such rules minimize the sum of the squared weights and, thereby, the sampling error (see the [Appendix](#)). Second, the more even distribution of the nodes

in QMC typically leads to lower numerical integration errors when compared to classical Monte Carlo integration, even though the integration is discontinuous, and we cannot expect the optimal QMC convergence order. On the other hand, higher order approaches, such as sparse grids,^{7,12} require a high degree of smoothness and, therefore, will likely be of no benefit. We are currently working on a more mathematical justification for the above arguments together with convergence proofs for the proposed estimator, which will be the subject of a subsequent publication.

In Sec. III, we target at the sensitivity of the expected turnover frequency from a kinetic Monte Carlo simulation. This means we are after a deterministic input–output relation as expectations carry no randomness. However, we need to estimate such expectations from a finite number of kMC simulations. The employed empirical averages necessarily carry some random error, and the CvM-GSA can only give the SInds of those averages. Employing the strategy from this section then ensures that the estimated SInd will converge against those SInds and that any deviation of the converged results from the targeted SInd is not due to a failure of the CvM estimator but only due to the approximation by empirical averages. In the language

TABLE I. Reaction mechanism for the CO oxidation on RuO₂(110) and corresponding nominal barriers E_a^α , as well as the ranges for the rate constants for a temperature of 600 K and CO and oxygen partial pressures of 1 bar.

Process	E_a^α (eV)	Rate constant (s ⁻¹)	Abbreviation
CO + * _{cus} → CO _{cus}	0.0	$2 \times [10^6, 10^8]$	CO ad. cus
CO + * _{br} → CO _{br}	0.0	$2 \times [10^6, 10^8]$	CO ad. br
O ₂ + 2 * _{cus} → O _{cus} + O _{cus}	0.0	$9.7 \times [10^5, 10^7]$	O ₂ ad. cus
O ₂ + 2 * _{br} → O _{br} + O _{br}	0.0	$9.7 \times [10^5, 10^7]$	O ₂ ad. br
O ₂ + * _{cus} + * _{br} → O _{br} + O _{cus}	0.0	$9.7 \times [10^5, 10^7]$	O ad. br/cus
CO _{cus} → CO + * _{cus}	1.3	$9.2 \times [10^4, 10^8]$	CO des. cus
CO _{br} → CO + * _{cus}	1.6	$2.8 \times [10^2, 10^6]$	CO des. br
O _{cus} + O _{cus} → O ₂ + 2 * _{cus}	2.0	$2.8 \times [10^{-1}, 10^3]$	O ₂ des. cus
O _{br} + O _{br} → O ₂ + 2 * _{br}	4.6	$4.1 \times [10^{-23}, 10^{-19}]$	O ₂ des. br
O _{br} + O _{cus} → O ₂ + * _{cus} + * _{br}	3.3	$3.4 \times [10^{-12}, 10^{-8}]$	O ₂ des. br/cus
CO _{cus} + * _{cus} → * _{cus} + CO _{cus}	1.7	$6.6 \times [10^{-4}, 1]$	CO diff. cus
CO _{br} + * _{br} → 217 * _{br} + CO _{br}	0.6	$1.1 \times [10^6, 10^{10}]$	CO diff. br
CO _{cus} + * _{br} → * _{cus} + CO _{br}	1.3	$1.5 \times [1, 10^4]$	CO diff. cus/br
CO _{br} + * _{cus} → * _{br} + CO _{cus}	1.6	$0.5 \times [10^{-2}, 10^2]$	CO diff. br/cus
O _{cus} + * _{cus} → * _{cus} + O _{cus}	1.6	$0.5 \times [10^{-2}, 10^2]$	O diff. cus
O _{br} + * _{br} → * _{br} + O _{br}	0.7	$1.6 \times [10^5, 10^9]$	O diff. br
O _{cus} + * _{br} → * _{cus} + O _{br}	1.0	$4.9 \times [10^2, 10^6]$	O diff. cus/br
O _{br} + * _{cus} → * _{br} + O _{cus}	2.3	$6.0 \times [10^{-9}, 10^{-5}]$	O diff. br/cus
CO _{cus} + O _{cus} → CO ₂ + 2 * _{cus}	0.9	$1.7 \times [10^3, 10^7]$	Ocus/COcus
CO _{br} + O _{br} → CO ₂ + 2 * _{cus}	1.5	$1.6 \times [10^{-2}, 10^2]$	Obr/CObr
CO _{cus} + O _{br} → CO ₂ + * _{br} + * _{cus}	1.2	$5.2 \times [1, 10^4]$	Obr/COcus
CO _{br} + O _{cus} → CO ₂ + * _{br} + * _{cus}	0.8	$1.2 \times [10^4, 10^8]$	Ocus/CObr

of this section, such deviations will only be due to drawing samples from a slightly different conditional distribution than the targeted.

III. NUMERICAL TESTS AND DISCUSSION

To be able to compare with our previous studies, we will demonstrate the methodology on the 1p-kMC model for the CO oxidation on $\text{RuO}_2(110)$ by Reuter and Scheffler.⁸ This is a very well investigated model,^{21–23} particularly in the context sensitivity analysis.^{6,14,24} Furthermore, the TOF is highly nonlinear in the considered parameter domain with close to discontinuous behavior, which makes it particularly suited for testing methodologies. This model considers bridge (br) and coordinately unsaturated (cus) sites that are arranged on a rectangular lattice in alternating rows and where CO and atomic oxygen can bind. On these sites, the model allows for dissociative oxygen adsorption and non-dissociative CO adsorption as well as the corresponding desorption processes. Furthermore, diffusion of adsorbed CO and O is considered between all neighboring sites. Adsorbed CO and O on adjacent sites can react to form gaseous CO_2 . The supporting data²⁵ contains the results of an additional simple model.

To make the results comparable, we considered exactly the same error model as in our previous study on W-GSA.⁶ This model is centered around the default settings for the reaction rate constants (RRC) at 600 K and CO and oxygen partial pressures of 1 bar using the rate expression and barriers from Ref. 8. As before, we assume a log-uniform distribution of all 22 RRC, which bounds are consistent with a possible error of ~ 0.25 eV for the reaction barriers. As a consequence, almost all RRCs can be up to a factor of 100 larger or lower than the default values, i.e., these RRCs can vary by four orders of magnitude. The only exceptions are the RRC for adsorption processes, which have a default barrier of zero. As negative barriers make no sense, these RRCs therefore can only be lower than the default values, and therefore, their uncertainty spans only two orders of magnitude. The list of all elementary reactions, default values for the barriers, the resulting ranges for the RRC, and the employed abbreviations are compiled in Table I.

Using this error model, we investigate the sensitivity of the stationary CO oxidation turnover frequency (TOF), i.e., the expected rate of CO molecules converted to CO_2 molecules normalized per surface unit cell. Numerical integration has been conducted using Sobol's Quasi-Monte Carlo (QMC) sequence²⁶ with up to $2^{17} \approx 1.3 \times 10^5$ nodes. For each node, an independent kMC simulation has been performed using the kMCOS toolbox^{27,28} using a lattice of 20×20 surface unit cells and 10^7 kMC steps each for relaxation to steady-state and subsequent time averaging amounting to ~ 10 CPU seconds per node and 300 CPU hours in total. Using this dataset, we find that the TOF varies within the covered domain of RRC by 12 orders of magnitude, i.e., between values of $\sim 10^{-6} \text{ s}^{-1}$ and $\sim 10^6 \text{ s}^{-1}$. Moreover, these values are no extreme outliers, but the marginal distribution of the TOF is very broad, showing a similarly high probability for a large range of possible TOF values. This becomes evident from Fig. 1, where we show the marginal density of $\log_{10}(\text{TOF})$ as obtained from a histogram with 28 bins for the range $\log_{10}(\text{TOF}) \in [-7, 7]$.

In Sec. III A, we test the approach with respect to its convergence with the number of quadrature nodes. Because the kMC estimates for the expected TOF of a given RRC are never perfect but

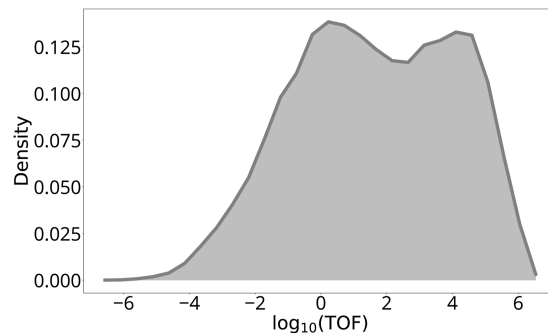


FIG. 1. Marginal density of $\log_{10}(\text{TOF})$ for the CO oxidation on $\text{RuO}_2(110)$, which has been obtained from a histogram with 28 bins for the range $\log_{10}(\text{TOF}) \in [-7, 7]$.

contain a sampling noise, we investigate the influence of noise on the final results in Sec. III B. In Sec. III D, we turn to the question of what is the effect if we modify the error distribution by reducing the error of one variable and/or correlating two variables.

A. Convergence

A crucial measure of the quality of a GSA approach is the convergence with the number of integration nodes N , i.e., with a total number of simulated kMC trajectories. Figure 2 displays this convergence for the proposed approach. The methodology will reach convergence when N approaches its maximum value. Most notably, the essential information can already be extracted at a comparatively low N of around a thousand, where the SInds deviate by a few percent from their converged numbers. This means we are able to conduct a GSA at a total cost in the order of a few CPU hours. These cost are comparable to or even below the computational effort that is needed to conduct a local sensitivity analysis for the very same 1p-kMC model using the advanced gradient estimation approaches.¹⁴ At these low N , we also get the relative importance of the different RRC correct, with CO des. cus having the most impact. This is followed by O_2 des. cus and CO ad. cus. O_2 ad. cus and Ocus/COcus sensitivities are a little lower and almost the same. We

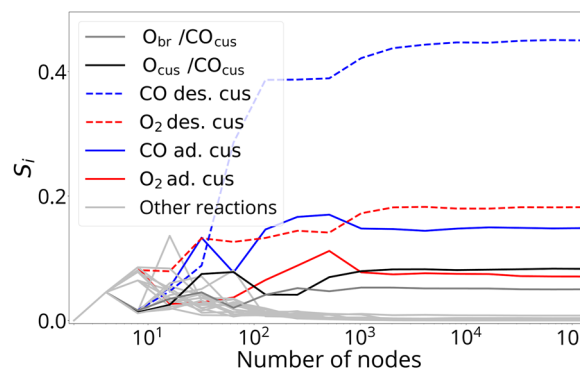


FIG. 2. Convergence with the number of QMC integration nodes. The stationary TOF has been obtained from kMC trajectories with 10^7 relaxation and sampling steps.

find the smallest SInd, which still differs significantly from zero, for the Obr/COcus reaction. All other SInds are close to zero. To investigate the influence of the kMC simulation settings, we have repeated the analysis with 10^8 relaxation and sampling steps per integration node. The convergence behavior is almost identical, and the final values for the SInd differ by less than 2%.

B. Noise tolerance

We are often interested in the sensitivity of an expected value, such as the stationary TOF in this study, i.e., the result that we would obtain if we average over, for a single quadrature node, infinitely many samples from our Monte Carlo model or an infinite trajectory for stationary data. In reality, we have to average over a finite number of samples or trajectories. Our estimates only approximate the true expected value and, therefore, always carry some random noise. If we conduct a GSA on the basis of these data, we are therefore addressing the sensitivity of these estimates and not that of the real expected values. We would expect that improving the accuracy per node would bring us closer to the SInd of the expected value.

Therefore, besides obtaining reasonable results with modest numbers of nodes, a critical factor for an efficient GSA of a Monte Carlo model is how accurately the model needs to be sampled at every quadrature point. A GSA method that is the least sensitive to such errors would allow a further reduction of the computational costs by running only cheap, low accurate simulations per node. To obtain an understanding of the effect of the sampling noise, we took our dataset and added independent, zero-mean Gaussian random noise $\alpha N(0, 1)$ to the TOF. Here, $N(0, 1)$ is a zero mean Gaussian noise with a standard deviation (STD) of 1 and α is the noise power. The results were rather disappointing, as can be seen in Fig. 3(a). Even modest noise, which STD is five orders of magnitude lower than the maximum TOF in our dataset, resulted in non-converging SInd. This seems to indicate that our methodology is useless and contradicts our findings where a recalculation of all results with 10^8 kMC steps produced almost indistinguishable results from the case with 10^7 steps. However, in kMC models, the sampling STD is not the same for each point in parameter space. We would rather expect it to be low when the expected TOF is low and high when the expected TOF is high. The simplest such noise model is relative noise, where the STD is proportional to the TOF. The results of adding this kind of noise $\alpha \text{TOF} N(0, 1)$ are shown in Fig. 3(b). Here, the noise power α is the ratio between the STD and the TOF, i.e., the inverse signal-to-noise ratio. The picture is now completely the opposite of the previous case. The correct SInd is reproduced for all noise powers, even when the noise is several orders of magnitude larger than the actual signal.

Motivated by this invariance, we tested how much we can decrease the number of sampling steps without affecting the CvM-GSA outcome. By this decrease, the sampling variance of our kMC estimates increases. While the sampling noise will not be purely relative noise, we expect this to hold approximately true and the SInd to be rather robust against a rather coarse sampling. The results for different numbers of sampling steps in the range $[10^2, 10^7]$ are displayed in Fig. 4. While the ideal behavior cannot be obtained, the results seem to be rather robust. Even for 10^3 steps, only minor quantitative deviations are obtained. Only if we lower the sampling even further, significant differences will show up. This is especially

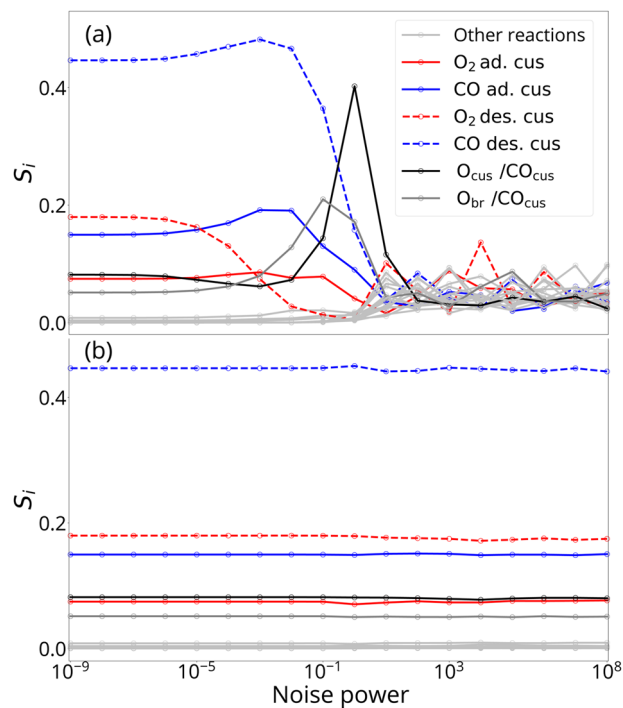


FIG. 3. Effect of adding independent zero-mean Gaussian noise to the TOF at each data point. (a) Independent zero-mean Gaussian noise, where the noise power is the standard deviation. (b) Relative zero-mean Gaussian noise, where the noise power is the proportionality constant between the standard deviation and the TOF.

remarkable as even for 10^7 sampling steps, the root-mean-square relative deviation from reference calculations with 10^8 sampling steps, i.e., a rough estimate for the average noise power, is already in the order of 10^{13} . This is, however, caused by only a few parameter points in our dataset; for 99%, the relative deviation is below one.

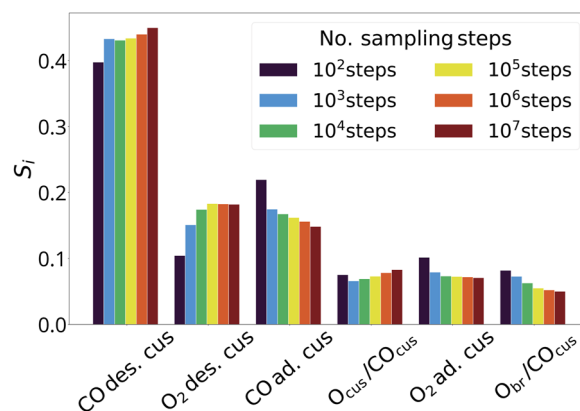


FIG. 4. The sensitivity indices by using different numbers of sampling steps for the elementary steps with significant SInd. Each group of bars corresponds to one elementary reaction, and the colors differentiate the employed number of sampling steps.

Thus, our data substantially deviate from the ideal relative noise behavior, but this is not such severe as to corrupt the performance of the approach.

Hence, we could reduce the computational time for sampling by 3–4 orders of magnitude compared to our nominal setting with 10^7 sampling steps. For the employed model, this cannot be translated into a significant reduction of the overall costs because for that, we need to also reduce the number of relaxation steps. This introduces a bias and leads to significant deviations already for 10^6 relaxation steps. For 10^5 relaxation steps, the most important parameter is then falsely identified. However, for many models, the relaxation is not as critical as the sampling as it is for the here employed kMC model. Using the same number of relaxation steps and sampling steps, the signal-to-noise ratio might then be substantially worse, and the above cases with artificially low numbers of samplings steps mimic this behavior. Thus, our results indicate that the methodology should also work for much more challenging cases. Examples, where high noise is expected in the target TOF are systems that require artificial slow down of the fastest processes, e.g., using acceleration schemes.^{29,30} In the supporting data,²⁵ we provide a simple example for a model, which allows the parallel reduction of relaxation and sampling steps.

C. Comparison with other methods

As already mentioned, the CvM lacks an intuitive interpretation, and it is therefore interesting to compare it with GSA approaches that possess such interpretation. In a previous study,⁶ we have developed the Wasserstein metric-based approach to GSA (W-GSA) and compared it with the main effect, which is the leading order term in a variance-based GSA.¹⁶ Both sensitivity indices possess the interpretation as a measure for the error in the output variable caused by the uncertainty of the respective input. These two approaches have been applied to the same 1p-kMC model and the same error model, as discussed in Subsections III A and III B. For comparison, we, however, have to note the slightly different footing of W-GSA and CvM-GSA. While both are based on some kind of distance between cumulative distributions, the Wasserstein metric is simply a norm, whereas the CvM is a squared norm. In Fig. 5, we, therefore, compare the results from CvM-GSA with the squared W-GSA and main effect for the $\log_{10}(\text{TOF})$ of CO oxidation on $\text{RuO}_2(110)$. In this representation, all three methods lead to the same picture. Only for the six displayed elementary steps, the SInds differ noticeably from zero and their values almost quantitatively agree between the three methods. Hence, CvM-GSA provides the same insight as the other two methods for the model at hand.

When it comes to numerical performance, CvM-GSA shows its advantages. All three methods work on a single set of QMC points. However, compared with the convergence results from our previous study,⁶ CvM-GSA shows a faster convergence with the number of QMC points, especially for those SInds that are close to zero when converged. Already at a few hundred points, the qualitative picture has been established with an accuracy that is comparable to the differences between the converged SInd from the three methods. It should also be noted that W-GSA and the main effect require an additional numerical discretization on top of the QMC integration. This discretization counteracts convergence with the number of QMC points, i.e., the more accurately we set this, the slower

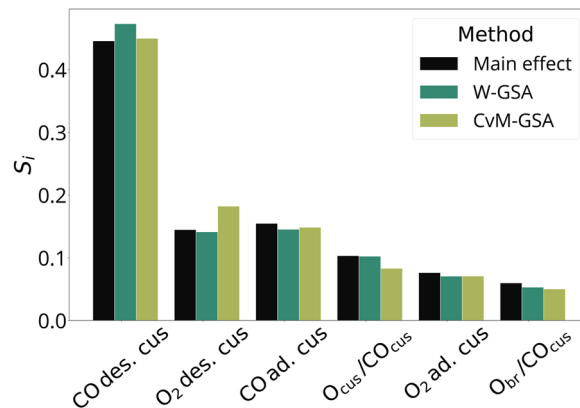


FIG. 5. Comparison of the CvM-GSA with Wasserstein metric based GSA and the variance based main Effect.⁶ Note that the later have been squared and subsequently normalized to ensure a somehow equal footing of all three methods. Therefore, the numbers deviate from Ref. 6.

the convergence will be, and both need to be balanced. In terms of robustness against noise in the simulation results, our tests showed very similar behavior for the normalized W-GSA, main effect, and CvM-GSA. The former two have here the slight disadvantage that the noise must be such that the TOF values stay positive due to the use of the logarithm.

Other approaches to GSA as the variance-based total sensitivity index¹⁶ or gradient-based GSA³¹ cannot be expected to be able to compete with CvM-GSA in the kMC setting. The direct sampling of the former requires an independent set of simulations for every SInd, which roughly multiplies the computational costs by the number of parameters.³² For the case at hand, CvM-GSA achieves a reasonable accuracy already with ~ 1000 simulations. For comparable costs, we would need to be able to estimate a SInd from as few as ~ 50 points. The challenge of gradient-based GSA is that parameter derivatives cannot be formulated as simple expected values in kMC (unlike equilibrium Monte Carlo). While there has been quite some progress in sampling approaches for such derivatives, these still require substantial computational efforts.³

D. Modifying the error distribution

We now turn to the question what is the effect if we change the error distribution. We look at the effect on the sensitivities and the distribution of the $\log_{10}\text{TOF}$ if we assume that we can reduce the uncertainty of a single barrier. We will also address the case when two barriers are correlated and the combination thereof with improving barriers. For demonstration purposes, we will only modify the (joint) distributions of the most important barrier, CO des. cus, and a single of the unimportant barriers, O diff. br/cus in Fig. 2. The errors for the remaining barriers remain independent of those two, obeying the original uniform distribution with a bound of 0.25 (eV). Reduced uncertainties are incorporated using Bayesian updates, i.e., it is assumed that they improve upon existing knowledge encoded in a prior distribution.³³ The density of the updated distribution is the product of the prior density and the likelihood, which encodes the additional knowledge.

Starting from the original error model as prior, we first investigate the case, when we improve a single barrier, either for O diff. br/cus or CO des. cus. For simplicity, we assume that these improved barriers take their nominal value and that we have an improved bound for their errors, which we set to 0.05 eV. Without no further information, the likelihood must be chosen proportional to an indicator function, which is one when the respective barrier is within $[-0.05, 0.05]$ eV around the nominal values and zero else. The resulting distribution is again uniform but now on the respective smaller domain. These domains are displayed in Fig. 6(a) in the plane spanned by $E_a^{\text{CO des. cus}}$ and $E_a^{\text{O diff. br/cus}}$ in dark turquoise and orange for the two cases. Such improved values might, for instance, come from higher fidelity quantum chemical methods or some kind of experiment. In any case, improved barriers come at substantial additional costs. Suppose now that we ignore the results from the GSA and, therefore, choose to improve O diff. br/cus. The resulting marginal density of the \log_{10} TOF and the effect on the sensitivity are shown in Figs. 7 and 8, respectively, using the same color code as in Fig. 6. For comparison, both figures also contain the results for the prior distribution in dark gray, i.e., the case that we

have investigated in Subsections III A–III D. For both, marginal distribution and SInd, the effect of the improved O diff. br/cus is negligible and the extra effort for improving this barrier was wasted. If we would instead follow the hierarchy of errors that results from the GSA, we would choose to improve the CO des. cus barrier. Now, the situation is much different and the marginal distribution in Fig. 7 is substantially changed. Interestingly, this does not reflect in the variance of \log_{10} (TOF), which remains almost unchanged at a value of 5.96.

This is due to the bimodal nature of the distribution and that, in our example, reducing the error has the effect that the probability weight is moved from intermediate to higher values of the TOF. However, we can argue that the uncertainty has been reduced because the probability weight now concentrates around these two modes, whereas the original distribution is more smeared out. Besides the marginal distribution, the SInd also changes significantly. The SInd of the CO des. cus is now almost negligible, which is to be expected because now the error of this barrier is very small. The qualitative picture of the remaining SInds does not change dramatically and suggests now putting the effort into determining either

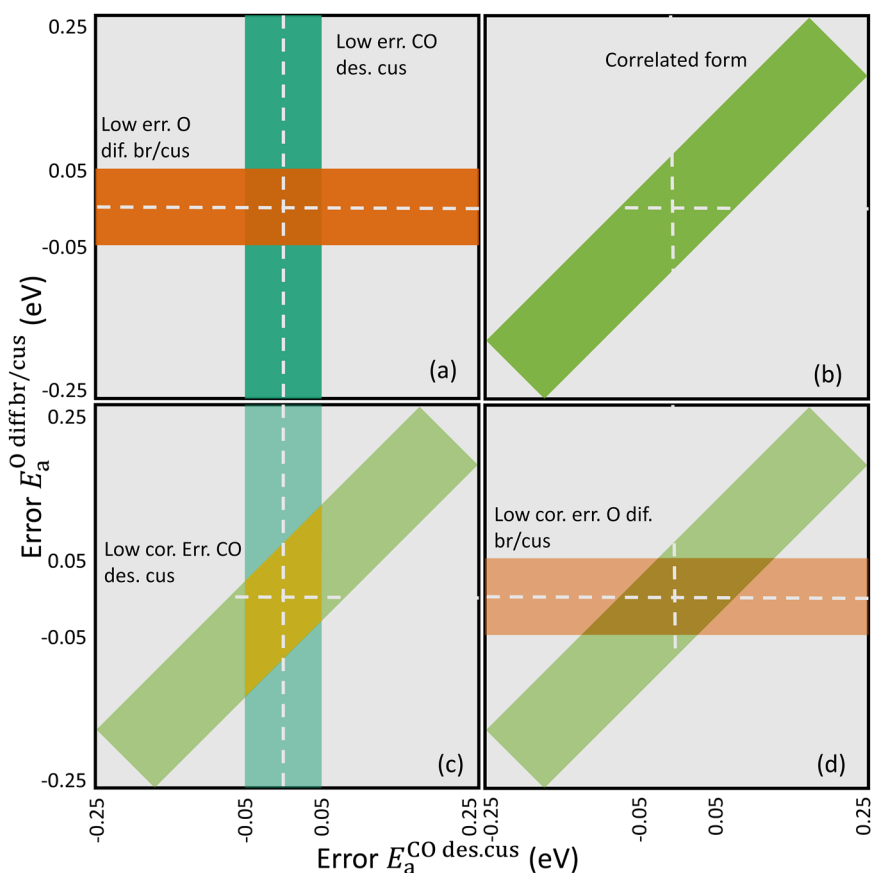


FIG. 6. Schematic representation of the modified error distributions for $E_a^{\text{CO des. cus}}$ and $E_a^{\text{O diff. br/cus}}$: (a) reduced uncertainty for $E_a^{\text{CO des. cus}}$ (orange) and $E_a^{\text{O diff. br/cus}}$ (dark turquoise), (b) correlated errors (green), (c) correlated errors with a reduced uncertainty of $E_a^{\text{CO des. cus}}$ (yellow), and (d) correlated errors with a reduced uncertainty of $E_a^{\text{O diff. br/cus}}$ (brown).

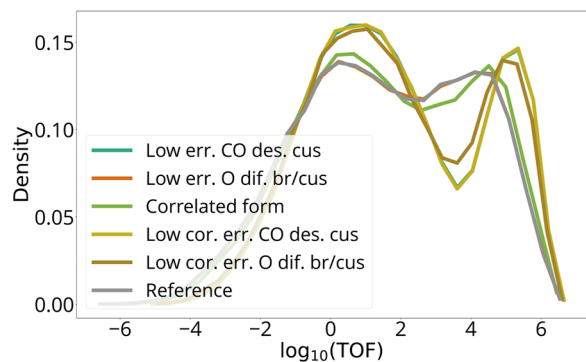


FIG. 7. Marginal densities of $\log_{10}(\text{TOF})$ for the different error models (cf. Fig. 6). The densities have been obtained from a histogram with 28 bins in the range $\log_{10}(\text{TOF}) \in [-7, 7]$.

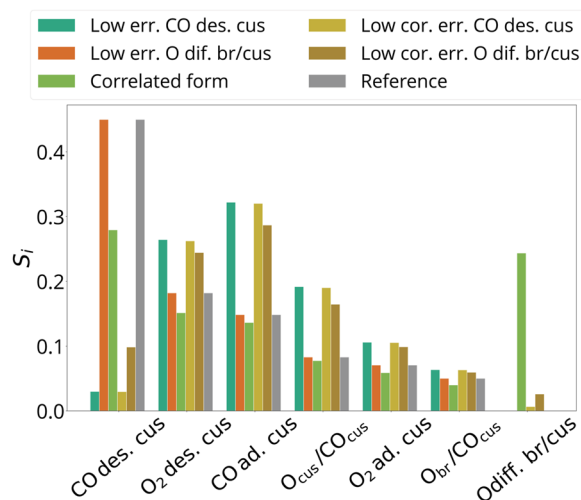


FIG. 8. CvM-GSA sensitivity indices for the different error models (cf. Fig. 6). Additionally, to the six most important steps in the uncorrelated reference case (cf. Fig. 4), the sensitivity with respect to the O dif. br/cus step was added.

the CO ad. cus or the O₂ des. cus/cus with higher accuracy instead of further improving upon CO des. cus.

We now consider that we have information on the statistical dependence between the errors of $E_a^{\text{CO des. cus}}$ and $E_a^{\text{O dif. br/cus}}$. To allow for a comparison with the original error model, we assume that this dependence is given by a uniform distribution, which support is displayed in Fig. 6(b) in light green. This distribution has the same bounds for the barriers as the original distribution and also the marginal distribution of a single barrier, respectively, the logarithm of the respective RC, are very close to uniform, else it encodes a strong dependence between the two barrier errors, where one error deviates from the other only within a rather small margin. Hence, the support of the distribution is a stripe, which width we have chosen to be 0.05 eV, and is essentially a rotated version of those from the previous two cases with lowered variance. The distribution of $\log_{10}(\text{TOF})$ in Fig. 7 hardly deviates from the uncorrelated case.

This is expected because one of the two correlated errors has no influence on the TOF when varied independently. The marginal distribution of $\log_{10}(\text{TOF})$ will not depend on whether we average over $E_a^{\text{O dif. br/cus}}$ or not, and the marginal distribution of the other errors is almost identical to the uncorrelated original case. In contrast to the marginal distribution, the SInds are strongly affected by the correlation, as shown in Fig. 8. Particularly, the sensitivity of CO des. cus is reduced, and we have now a large sensitivity on the O dif. br/cus of almost the same value. This importance of the O dif. br/cus arises because if we know the value of this barrier, we also know the barrier of the CO des. cus within a narrow margin because of the statistical dependence between the two. Since the TOF is most sensitive to the latter already in the original case, this leads to a sensitivity with respect to the O dif. br/cus in the correlated case.

To investigate the effect of improved uncertainties in the presence of correlation, we have repeated the experiments with lowered uncertainties for $E_a^{\text{CO des. cus}}$ and $E_a^{\text{O dif. br/cus}}$ but now using the correlated distribution [cf. Fig. 6(b)] as prior. The support of the resulting distributions is displayed in yellow in Fig. 6(c) for a reduced error of $E_a^{\text{CO des. cus}}$ and in brown in Fig. 6(d) for a reduced error of $E_a^{\text{O dif. br/cus}}$, respectively. For the case with the reduced error of $E_a^{\text{CO des. cus}}$, we observe that the marginal distributions of the $\log_{10}(\text{TOF})$ in Fig. 7 using the correlated and uncorrelated priors, respectively, agree perfectly and also the effect on the sensitivity is almost identical. The reason for this is again that averaging or not over $E_a^{\text{O dif. br/cus}}$ has no influence, and the marginal distribution of the other errors is identical for the uncorrelated case. In contrast, the correlation between the two barriers induces a lower uncertainty of $E_a^{\text{CO des. cus}}$ when the uncertainty of $E_a^{\text{O dif. br/cus}}$ is reduced. This is reflected in Fig. 6(d) where the support of the distribution extends much less in the $E_a^{\text{CO des. cus}}$ -direction in the correlated case without improved uncertainties. As a consequence, the uncorrelated and the correlated case significantly differ for a reduced error of $E_a^{\text{O dif. br/cus}}$. In particular, the latter rather resembles the cases with a lowered error of $E_a^{\text{CO des. cus}}$ than the former (cf. Figs. 7 and 8). However, the marginal distribution of $E_a^{\text{CO des. cus}}$ encodes a slightly higher uncertainty of $E_a^{\text{CO des. cus}}$ than when directly introducing the bounds for $E_a^{\text{CO des. cus}}$. Therefore, the effect on the distribution of $\log_{10}(\text{TOF})$ and the sensitivity is slightly less pronounced. To some extent, this is expected because for the correlated case without improved uncertainties, the O dif. br/cus has a smaller SInd than the CO des. cus. Thus, the correlation induced sensitivity is not simply an artifact but is fully consistent with the very purpose of sensitivity analysis, namely, to identify factors, for which an improved accuracy reduces the uncertainty of the model output.

IV. CONCLUSION

We have presented an approach to the global sensitivity analysis of Monte Carlo models on the basis of the Cramér–von Mises distance and demonstrated its value on a 1p-kMC model for CO oxidation on RuO₂(110). It is purely based on numerical integration and can be implemented with a few lines of code. Comparing with other approaches to global sensitivity, the new approach delivers very comparable results, while it is more efficient in terms of the number of required 1p-kMC simulations and particularly easy to

use. Moreover, it also seems to be very robust against kMC sampling noise and sufficient accuracy can be obtained already with very inaccurate kMC sampling and large noise to signal ratios. Both together pave the way to the computationally efficient treatment of very challenging models where it is difficult to obtain accurate simulation results, which would be needed for more classical approaches to sensitivity analysis.

Besides testing efficiency, we have investigated the effect of changing the underlying error distribution mimicking selective reduction of parameter errors, error correlation, and a combination thereof. In all cases, the approach showed the expected behavior, namely, to identify those parameters for which the reduction of the respective error has the most positive impact on the accuracy of the model's output.

Future improvement might employ randomized quadrature rules such that the quadrature error in the SInd can be estimated using statistical approaches. Open points, which we currently investigate, are a proof of the invariance under relative noise and convergence rates for the proposed estimator with general quadrature rules.

ACKNOWLEDGMENTS

This work was funded by the Deutsche Forschungsgemeinschaft (DFG, German Research Foundation) under Germany's Excellence Strategy–EXC 2008–390540038–UniSysCat and by the CRC 1114 “Scaling Cascades in Complex Systems” funded by the Deutsche Forschungsgemeinschaft (Project ID: 235221301). The authors acknowledge the computing resources provided by the Max Planck Computing and Data Facility.

AUTHOR DECLARATIONS

Conflict of Interest

The authors have no conflicts to disclose.

Author Contributions

Sina Dortaj: Conceptualization (equal); Data curation (lead); Formal analysis (equal); Methodology (equal); Software (lead); Visualization (lead); Writing – original draft (supporting). **Sebastian Matara:** Conceptualization (equal); Formal analysis (lead); Funding acquisition (lead); Methodology (equal); Supervision (lead); Writing – original draft (equal).

DATA AVAILABILITY

The 1p-kMC simulation data and sample code for CvM-GSA are available from the Edmond Open Research Data Repository of the Max Planck Society.²⁵ This also contains results for an additional simple model.

APPENDIX: INTEGRATION OF MONTE CARLO MODELS

The estimator for the CvM requires to numerically solve integrals I of the type

$$\begin{aligned} I &:= \int t(y, \mathbf{x}) dF(y, \mathbf{x}) \\ &= \iint t(y, \mathbf{x}) dF(y|\mathbf{x}) dF(\mathbf{x}) \\ &= \int E_{y|\mathbf{x}}(t(y, \mathbf{x})) dF(\mathbf{x}), \end{aligned} \quad (\text{A1})$$

where $dF(y, \mathbf{x})$ is the measure for the joint distribution $F(y, \mathbf{x})$ of output y and input \mathbf{x} introduced in Sec. II. Correspondingly, $dF(\mathbf{x})$ is the measure of the distribution $F(\mathbf{x})$ of only the input \mathbf{x} and $dF(y|\mathbf{x})$ is the measure of the distribution $F(y|\mathbf{x})$ of the output y conditioned on the input \mathbf{x} . The conditional expectation $E_{y|\mathbf{x}}(t(y, \mathbf{x})) = \int t(y, \mathbf{x}) dF(y|\mathbf{x})$ is a function of the input \mathbf{x} . For the following, we want to assume that the conditional variance is bounded by an (unknown) constant V , i.e.,

$$\text{Var}_{y|\mathbf{x}}(t(y, \mathbf{x})) = \int t(y, \mathbf{x})^2 - E_{y|\mathbf{x}}(t(y, \mathbf{x}))^2 dF(y|\mathbf{x}) \leq V, \quad \forall \mathbf{x}, \quad (\text{A2})$$

which holds for the integral formulation of the marginal CDFs (1)–(3) and also for the CvM because in both cases, the integrands are bounded and therefore the conditional variance. For the case that we estimate the CvM using the approximate CDFs (9)–(11), this bounding can be guaranteed if these are obtained from quadrature rules with positive weights. For general rules, the approximate CDFs can, in principle, take arbitrary positive and negative values, depending on the problem and the employed rule.

We assume no explicit knowledge on $F(y|\mathbf{x})$ and only require a (Monte Carlo) model that draws statistically independent samples from $F(y|\mathbf{x})$ for a given \mathbf{x} . To obtain a numerical estimate of the integral, we suppose that we have a quadrature rule with N nodes $\{\mathbf{x}_n\}_{n=1}^N$ and weights $\{w_n\}_{n=1}^N$ for the integration over the distribution of the input parameters $F(\mathbf{x})$, for which

$$\sum_{n=1}^N w_n = 1, \quad (\text{A3})$$

$$\lim_{N \rightarrow \infty} \sum_{n=1}^N s(\mathbf{x}_n) w_n = \int s(\mathbf{x}) dF(\mathbf{x}), \quad (\text{A4})$$

$$\lim_{N \rightarrow \infty} |w_n|^2 = 0 \quad (\text{A5})$$

hold all N and for any reasonable $s(\mathbf{x})$, especially for $s(\mathbf{x}) = E_{y|\mathbf{x}}(t(y, \mathbf{x}))$. We employ the (Monte Carlo) model to draw a single sample y_n from $F(y|\mathbf{x}_n)$ for each node \mathbf{x}_n . Then, the estimator

$$\tilde{I}_N = \sum_{n=1}^N t(y_n, \mathbf{x}_n) w_n \quad (\text{A6})$$

converges against the true integral, and its expected square error is bounded by

$$E[(I - \tilde{I}_N)^2] \leq (I - I_N)^2 + V \sum_{n=1}^N w_n^2, \quad (\text{A7})$$

where the expectation is taken with respect to the randomness of output samples $\{y_n\}_{n=1}^N$ and

$$I_N := \sum_{n=1}^N E_{y|x_n}(t(y, \mathbf{x}_n)) w_n \quad (\text{A8})$$

is the numerical approximate of the integral I if we could perform the inner expectation exactly. Convergence follows then from the bound (A7) and that $(I - I_N)^2$ and $\sum_{n=1}^N w_n^2$ converge against zero for $N \rightarrow \infty$.

Proof of the error bound (A7): To prove the error bound, we decompose the expected square deviation between the true integral I and the estimator \tilde{I}_N ,

$$\begin{aligned} E[(I - \tilde{I}_N)^2] &= E[(I - I_N + I_N - \tilde{I}_N)^2] \\ &= (I - I_N)^2 + \text{Var}(\tilde{I}_N) \\ &= (I - I_N)^2 + \sum_{n=1}^N w_n^2 \text{Var}_{y|x_n}(t(y, \mathbf{x}_n)) \\ &\leq (I - I_N)^2 + V \sum_{n=1}^N w_n^2, \end{aligned} \quad (\text{A9})$$

where in the first line, we added a zero $I_N - I_N$ and exploited for the second line that I_n is the expected value of \tilde{I}_n . The third line results from explicitly formulating the latter. The subsequent inequality arises from exploiting the upper bound for the conditional variance (A2). $(I - I_N)^2$ represents the numerical error due to the discretization using a quadrature rule of finitely many nodes $\{\mathbf{x}_n\}_{n=1}^N$. Correspondingly, $\text{Var}(\tilde{I}_N) \leq V \sum_{n=1}^N w_n^2$ is the sampling error due to using just a single sample y_n per node. Among all possibilities, equal weight quadrature rules minimize the bound $V \sum_{n=1}^N w_n^2$ for the sampling error, which then becomes V/N . Thus, these are particularly suited for estimating such integrals and, in higher dimensions, we would therefore choose random Monte Carlo or quasi-Monte Carlo for numerical quadrature. For dimensionality in the order of few tens, quasi-Monte Carlo rules are the method of choice if we can map $F(\mathbf{x})$ onto a uniform distribution on a hypercube. For such cases, they typically perform better than usual Monte Carlo integration rules because the nodes cover the cube more evenly. For deterministic models (or low V) and smooth integrands $t(y, \mathbf{x})$, higher order rules with unequal weights might be better suited, e.g., sparse grids. For the problem at hand, $t(y, \mathbf{x})$ cannot be considered smooth, and thus, quasi-Monte Carlo is the method of choice.

REFERENCES

- ¹IUPAC. *Compendium of Chemical Terminology*, 2nd ed., compiled by A. D. McNaught and A. Wilkinson, (Blackwell Scientific Publications, Oxford, 1997), ISBN 0-9678550-9-8; online version created by S. J. Chalk, <https://doi.org/10.1351/goldbook>.
- ²C. T. Campbell, "The degree of rate control: A powerful tool for catalysis research," *ACS Catal.* **7**, 2770–2779 (2017).
- ³S. Matera, W. F. Schneider, A. Heyden, and A. Savara, "Progress in accurate chemical kinetic modeling, simulations, and parameter estimation for heterogeneous catalysis," *ACS Catal.* **9**, 6624–6647 (2019).
- ⁴J. Feng, J. Lansford, A. Mironenko, D. B. Pourkargar, D. G. Vlachos, and M. A. Katsoulakis, "Non-parametric correlative uncertainty quantification and sensitivity analysis: Application to a Langmuir bimolecular adsorption model," *AIP Adv.* **8**, 035021 (2018).
- ⁵J. E. Sutton and D. G. Vlachos, "Effect of errors in linear scaling relations and Bronsted–Evans–Polanyi relations on activity and selectivity maps," *J. Catal.* **338**, 273–283 (2016).
- ⁶S. Döpking and S. Matera, "Error propagation in first-principles kinetic Monte Carlo simulation," *Chem. Phys. Lett.* **674**, 28–32 (2017).
- ⁷A. Alexanderian, F. Rizzi, M. Rathinam, O. P. Le Maître, and O. M. Knio, "Preconditioned Bayesian regression for stochastic chemical kinetics," *J. Sci. Comput.* **58**, 592–626 (2014).
- ⁸K. Reuter and M. Scheffler, "First-principles kinetic Monte Carlo simulations for heterogeneous catalysis: Application to the CO oxidation at RuO₂(110)," *Phys. Rev. B* **73**, 045433 (2006).
- ⁹M. Pineda and M. Stamatakis, "Kinetic Monte Carlo simulations for heterogeneous catalysis: Fundamentals, current status, and challenges," *J. Chem. Phys.* **156**, 120902 (2022).
- ¹⁰M. Andersen, C. Panosetti, and K. Reuter, "A practical guide to surface kinetic Monte Carlo simulations," *Front. Chem.* **7**, 202 (2019).
- ¹¹A. Bruix, J. T. Margraf, M. Andersen, and K. Reuter, "First-principles-based multiscale modelling of heterogeneous catalysis," *Nat. Catal.* **2**, 659–670 (2019).
- ¹²S. Döpking, C. P. Plaisance, D. Strobusch, K. Reuter, C. Scheurer, and S. Matera, "Addressing global uncertainty and sensitivity in first-principles based microkinetic models by an adaptive sparse grid approach," *J. Chem. Phys.* **148**, 034102 (2018).
- ¹³T. De Wet, "Cramér-von Mises tests for independence," *J. Multivar. Anal.* **10**, 38–50 (1980).
- ¹⁴M. J. Hoffmann, F. Engelmann, and S. Matera, "A practical approach to the sensitivity analysis for kinetic Monte Carlo simulation of heterogeneous catalysis," *J. Chem. Phys.* **146**, 044118 (2017).
- ¹⁵E. Plischke, E. Borgonovo, and C. L. Smith, "Global sensitivity measures from given data," *Eur. J. Oper. Res.* **226**, 536–550 (2013).
- ¹⁶A. Saltelli, M. Ratto, T. Andres, F. Campolongo, J. Cariboni, D. Gatelli, M. Saisana, and S. Tarantola, "Variance-based methods," in *Global Sensitivity Analysis. the primer* (John Wiley & Sons, Ltd., 2007), Chap. 4, pp. 155–182.
- ¹⁷J. E. Sutton, W. Guo, M. A. Katsoulakis, and D. G. Vlachos, "Effects of correlated parameters and uncertainty in electronic-structure-based chemical kinetic modelling," *Nat. Chem.* **8**, 331–337 (2016).
- ¹⁸G. E. B. Archer, A. Saltelli, and I. M. Sobol, "Sensitivity measures, ANOVA-like techniques and the use of bootstrap," *J. Stat. Comput. Simul.* **58**, 99–120 (1997).
- ¹⁹F. Gamboa, T. Klein, and A. Lagnoux, "Sensitivity analysis based on Cramér-von Mises distance," *SIAM/ASA J. Uncertainty Quantif.* **6**, 522–548 (2018).
- ²⁰P. L'Ecuyer, "Randomized quasi-Monte Carlo: An introduction for practitioners," in *Monte Carlo and Quasi-Monte Carlo Methods*, edited by A. B. Owen and P. W. Glynn (Springer International Publishing, Cham, 2018), pp. 29–52.
- ²¹P. Gelß, S. Matera, and C. Schütte, "Solving the master equation without kinetic Monte Carlo: Tensor train approximations for a CO oxidation model," *J. Comput. Phys.* **314**, 489–502 (2016).
- ²²F. Hess, A. Farkas, A. P. Seitsonen, and H. Over, "First-principles" kinetic Monte Carlo simulations revisited: CO oxidation over RuO₂(110)," *J. Comput. Chem.* **33**, 757–766 (2012).
- ²³H. Wang, T. Shen, and X. Xu, "A good prediction of the overall reaction rate may not mean a correct description of the reaction kinetics: A case study for CO oxidation on RuO₂(110) surfaces," *J. Phys. Chem. C* **125**, 9169–9177 (2021).
- ²⁴H. Meskine, S. Matera, M. Scheffler, K. Reuter, and H. Metiu, "Examination of the concept of degree of rate control by first-principles kinetic Monte Carlo simulations," *Surf. Sci.* **603**, 1724–1730 (2009).
- ²⁵S. Matera, (2023) "Supplementary material for efficient global sensitivity analysis of kinetic Monte Carlo simulations using Cramér von Mises distance," Edmond Open Research Data Repository. Edmond Open Research Data Repository. <https://doi.org/10.17617/3.EPRBFA>.
- ²⁶I. Sobol', "On the distribution of points in a cube and the approximate evaluation of integrals," *USSR Comput. Math. Math. Phys.* **7**, 86–112 (1967).
- ²⁷M. J. Hoffmann, S. Matera, and K. Reuter, "Kmos: A lattice kinetic Monte Carlo framework," *Comput. Phys. Commun.* **185**, 2138–2150 (2014).
- ²⁸See <https://github.com/kmos> for Kmos software.

²⁹E. C. Dybeck, C. P. Plaisance, and M. Neurock, “Generalized temporal acceleration scheme for kinetic Monte Carlo simulations of surface catalytic processes by scaling the rates of fast reactions,” *J. Chem. Theory Comput.* **13**, 1525–1538 (2017).

³⁰T. Danielson, J. E. Sutton, C. Hin, and A. Savara, “SQERTSS: Dynamic rank based throttling of transition probabilities in kinetic Monte Carlo simulations,” *Comput. Phys. Commun.* **219**, 149–163 (2017).

³¹I. Sobol and S. Kucherenko, “Derivative based global sensitivity measures and their link with global sensitivity indices,” *Math. Comput. Simul.* **79**, 3009–3017 (2009).

³²F. Campolongo, A. Saltelli, and J. Cariboni, “From screening to quantitative sensitivity analysis. A unified approach,” *Comput. Phys. Commun.* **182**, 978–988 (2011).

³³D. V. Lindley, “Bayesian statistics a review,” *Bayesian Statistics* (SIAM, 1972), pp. 1–74.